The *n*th Power Fourier Spectrum Analysis for the Generalized Seismic Wavelets

Xuan Ke, Ying Shi, Xiaofei Fu, Liwei Song, Hongliang Jing, Jingbo Yang, and Zhen Zhang

***Abstract*— The generalized seismic wavelets (GSWs) are defined by fractional derivatives of the Gaussian function, whose asymmetry allows them to represent seismic signals more accurately than the commonly used symmetrical Ricker wavelet. The latter is a particular case with a second derivative of the Gaussian function. To better obtain the GSW, which could be well-matched with seismic signals, this article proposes the *n*th power Fourier spectrum analysis method for GSWs. First, based on the *n*th power Fourier spectrum of GSWs, the proposed method builds the mathematical relationship between the frequency characteristics (e.g., central frequency and bandwidth) and the statistical properties (e.g., mean frequency and deviation). Second, according to the *n*th power Fourier spectrum, we propose a weighting calculation method for the derivative order *u* of the Gaussian function. This method could be used for estimating GSWs matched the seismic first-arrival record, which is conducive to improving the accuracy of seismic imaging, inversion, and *Q* analysis. In theory, our proposed weighting method has better robustness and noise resistance than the traditional spectrum analysis method based on the power or amplitude spectrum. The experiment of synthetic noise, including first-arrival record and vertical seismic profiling (VSP) field data, shows the effectiveness of the proposed approach.**

***Index Terms*— Generalized seismic wavelets (GSWs), *n*th power Fourier spectrum, numerical solution.**

Manuscript received 16 September 2022; revised 21 December 2022; accepted 4 February 2023. Date of publication 8 February 2023; date of current version 28 February 2023. This work was supported in part by the Project of the National Natural Science Foundation of China under Grant 41930431, Grant 41974116, Grant 42274171, and Grant 41904121; in part by the Outstanding Youth Project of Natural Science Foundation of Heilongjiang under Grant YQ2021D008; in part by China National Petroleum Corporation (CNPC) Innovation Fund under Grant 2021DQ02-0302; in part by the China Postdoctoral Science Foundation under Grant 2019M651253; in part by the Heilongjiang Provincial Postdoctoral Science Foundation under Grant LBH-Z18040; in part by the "Key Laboratory of Formation Mechanism and Resource Evaluation of Oil and Gas Reservoirs in Heilongjiang Province" Open Fund Project under Grant KL20190105; in part by the Pilot Innovation Fund of Northeastern Petroleum University under Grant 2021YDL-04; and in part by the Universities Reformation and Development Personnel Training Supporting Project from Central Authorities under Grant 140119001. *(Corresponding author: Xuan Ke.)*

Xuan Ke and Ying Shi are with the School of Earth Science, the Key Laboratory of Oil and Gas Reservoir Formation Mechanism and Resource Evaluation, and the Key Laboratory of Continental Shale Hydrocarbon Accumulation and Efficient Development, Ministry of Education, Northeast Petroleum University, Daqing 163318, China, also with the Heilongjiang Provincial Key Laboratory of Oil and Gas Geophysical Exploration, Daqing 163318, China, and also with the National Engineering Research Center of Offshore Oil and Gas Exploration, Beijing 100027, China (e-mail: kexuan@nepu.edu.cn; shiying@nepu.edu.cn).

Xiaofei Fu is with the Institute of Unconventional Oil and Gas, Northeast Petroleum University, Daqing 163318, China (e-mail: 760136897@qq.com).

Liwei Song is with the School of Physics and Electronic Engineering, Northeast Petroleum University, Daqing 163318, China (e-mail: zhidao90@163.com).

Hongliang Jing is with the Research and Development Center, BGP Inc., CNPC, Zhuozhou 072750, China (e-mail: jinghongliang@cnpc.com.cn).

Jingbo Yang is with the Exploration Division, PetroChina Tarim Oilfield Company, Korla 841000, China (e-mail: yjingb-tlm@petrochina.com.cn).

Zhen Zhang is with the Research Institute of Exploration and Development, PetroChina Tarim Oilfield Company, Korla 841000, China (e-mail: zzhen-tlm@petrochina.com.cn).

Digital Object Identifier 10.1109/TGRS.2023.3243184

I. Introduction

RICKER wavelet proposed by Ricker [1], [2], [3] has been widely used for seismic data processing. However, the symmetrical waveform of the Ricker wavelet is rare in nature. In addition, its definition and application of frequency parameters are still controversial [4]. In practice, wavelets that are well-matched to field signals often play essential roles in seismic data analysis, such as stable Q analysis [5], [6], seismic data modeling [7], [8], [9], reverse time migration [10], [11], [12], [13], [14], and full-waveform inversion [15], [16], [17]. The simple symmetrical Ricker wavelet is unsuitable for these applications. So, more generalized wavelets should be adopted to achieve better results in seismic data processing.

Effective seismic wavelet estimation methods can help address the problems mentioned above. Generally, these methods can be divided into two main categories: deterministic and statistical. Deterministic methods need to combine with well data [18] and are typically solved using least-squares or spectral division methods [19], [20]. Statistical methods, on the other hand, estimate the seismic wavelet from the seismic data alone [21]. However, the Earth's response can influence the statistical properties of the wavelet unpredictably. To address this issue, geophysicists have proposed several approaches to enhance the robustness of wavelet estimation methods [22], [23], [24], [25].

Wang [26] proposed a mathematical model for constructing seismic wavelets called generalized seismic wavelets (GSWs). They are defined by various derivatives of a Gaussian potential function and show various waveforms in the time domain, which are conducive to matching the seismic recording. In the frequency domain, the different derivatives of the Gaussian function could be understood as the Gaussian spectrum multiplied by a frequency-related factor ω^u, where ω is the angular frequency and u is the order of the derivative. This characteristic in the frequency domain can physically represent the frequency-dependent attenuation of the seismic wave when propagating through viscoelastic media. This demonstrates that the GSWs are suitable for estimating the field wavelet signals both mathematically and physically. Furthermore, GSWs have also been recently used for calculating the depth-domain

seismic wavelet [25], detecting Karst voids based on dominant frequencies of seismic profiles [27], and estimating the Q-factor [28]. Therefore, research on GSW extraction methods with more stability and noise resistance positively impacts seismic data processing.

Frequency analysis is a classical approach for estimating the best-matched wavelets with seismic recording and extracting the frequency parameters. In general, amplitude [29], [30], [31] and power spectra [32] are commonly used in frequency analysis, because they have clear physical meaning. Among them, with the help of the Lambert W function [33], [34], the power spectrum analysis method of the GSW proposed by Wang [35] clearly illustrates the mathematical relationship between the frequency characteristics and statistical properties. However, this analysis method only focuses on the amplitude and power spectra, which are the first and quadratic power of the modulus of Fourier spectra. It is not sufficiently generalized to consider other power numbers of the Fourier spectrum. Additionally, using a single-power-spectrum analysis method may introduce errors when the data contains noise. To address these issues, this article extends the spectrum analysis method of the GSW [26] from the power spectrum analysis to the nth power Fourier spectrum analysis. By introducing an arbitrary power number n of the Fourier spectrum, this article deduces the clear mathematical relationship between the frequency characteristics and statistical properties, in which the latter depends on both the derivative order of the Gaussian function and the power number n of the Fourier spectrum. This means that the arbitrary nth power Fourier spectrum could be used for analyzing the frequency as well as estimating and matching the GSW with the seismic signals, not limited to using the amplitude or power spectrum. More importantly, according to the proposed weighting method, the potential error of using a single-power-spectrum analysis method can be avoided considering the spectrum analysis results of different power orders. Additionally, the proposed method allows for accurately determining the power number n for the GSW, ensuring that the mean and central frequencies are almost equal. This is a theoretical extension of Wang's [26] viewpoint that the mean frequency obtained by the power spectrum is closer to the central frequency of the wavelet than the one received by the amplitude spectrum [36]. At last, the effectiveness of the proposed measure is finally verified through wavelet estimation for synthetic first arrival record with noise and vertical seismic profiling (VSP) field data.

This article includes five sections in addition to the introduction.

1) Section II mainly reviews the GSW and frequency characteristics which serve as the theoretical background of this article.

2) Section III introduces the theory of nth power Fourier spectrum analysis for the GSW, which establishes the mathematical relationship between the frequency characteristics and statistical properties of the nth power Fourier spectrum.

3) Section IV tells the weighting algorithm of the nth power Fourier spectrum, which provides the theoretical guidance for the practical application of this method.

4) Section V includes synthetic and field examples to demonstrate the validity of our method.

5) Section VI offers conclusion and discussions about the proposed method.

II. GSWs and Frequency Characteristics

This section mainly reviews the GSW and the power spectrum analysis proposed by Wang [26]. First, a potential function in negative Gaussian is introduced as follows:

$$g(\tau) = -\sqrt{\pi}\omega_0 \exp\left[-\frac{\omega_0^2}{4}(\tau-\tau_0)^2\right] \tag{1}$$

where τ represents time in s, τ_0 is the parameter to adjust the time position of the symmetrical axis, and ω_0 denotes the reference angular frequency, which is in rad/s.

The GSW could be expressed as the fractional derivatives of the negative Gaussian in the time domain [37]

$$g^{(u)}(\tau) = \frac{1}{\Gamma(m-u)}\int_0^{\tau}(\tau-\xi)^{m-u-1}g^{(m)}(\xi)d\xi \tag{2}$$

where m is an integer and $g^{(m)}$ is the mth-order partial derivative of $g(\tau)$ with respect to τ. u is a fraction between $[m-1, m)$, and $g^{(u)}(\tau)$ is the uth fraction-order partial derivative of $g(\tau)$ with respect to τ. $\Gamma()$ represents the Gamma function. When the reference frequency ω_0 and the time position parameter τ_0 are given, with the change in the partial derivative order u, the GSW could be shown as the waveform with different phases, which can help the GSW match the seismic trace record in the time domain.

The normalized spectrum and the amplitude spectrum of the GSW educed with the Fourier transform could be expressed as follows [26]:

$$\Phi^{(u)}(\omega) = \left(\frac{u}{2}\right)^{-\frac{u}{2}}\frac{\omega^u}{\omega_0^u}\exp\left(-\frac{\omega^2}{\omega_0^2}+\frac{u}{2}\right) \times \exp\left[-i\omega\tau_0 + i\pi\left(1+\frac{u}{2}\right)\right] \tag{3}$$

$$|\Phi^{(u)}(\omega)| = \left(\frac{u}{2}\right)^{-\frac{u}{2}}\frac{\omega^u}{\omega_0^u}\exp\left(-\frac{\omega^2}{\omega_0^2}+\frac{u}{2}\right). \tag{4}$$

If the derivative of the amplitude spectrum $|\Phi^{(u)}(\omega)|$ with respect to the frequency ω is set to zero, after some derivations, the peak frequency could be expressed as follows:

$$\omega_p = \omega_0\sqrt{\frac{u}{2}}. \tag{5}$$

Setting the amplitude is as 1/2 and by substituting it into (4), we can obtain the following:

$$\left(\frac{2}{u}\right)^{\frac{u}{2}}\frac{\omega^u}{\omega_0^u}\exp\left(-\frac{\omega^2}{\omega_0^2}+\frac{u}{2}\right) = \frac{1}{2}. \tag{6}$$

After some derivations, (6) could be rewritten as follows:

$$-\frac{2}{u}\frac{\omega^2}{\omega_0^2}\exp\left(-\frac{2}{u}\frac{\omega^2}{\omega_0^2}\right) = -\frac{1}{2^{2/u}e} \tag{7}$$

where e is the Euler number and (7) could be seen as an inverse exponential equation form as follows:

$$zexp(z) = x. \tag{8}$$

The Lambert W function could be introduced to solve (8) [26], [34], [35], [38]

$$z = W(x). \tag{9}$$

Therefore, the solution of (7) is

$$W\left(-\frac{1}{2^{2/u}e}\right) = -\frac{2}{u}\frac{\omega^2}{\omega_0^2}. \tag{10}$$

For $x = -1/(2^{2/u}e) < 0$, the Lambert W function has two branches: $W_{-1}(x) \le -1$ and $W_0(x) \ge -1$. Therefore, we could obtain the analytic solution of (10) on each of the two Lambert W function branches as follows:

$$\omega_{l1} = \omega_0\sqrt{-\frac{u}{2}W_0\left(-\frac{1}{2^{2/u}e}\right)} \tag{11}$$

$$\omega_{l2} = \omega_0\sqrt{-\frac{u}{2}W_{-1}\left(-\frac{1}{2^{2/u}e}\right)}. \tag{12}$$

From which, the half-bandwidth ω_b and the center of the frequency band ω_c could be determined as follows:

$$\omega_c = \frac{\omega_0}{2}\left[\sqrt{-\frac{u}{2}W_{-1}\left(-\frac{1}{2^{2/u}e}\right)} + \sqrt{-\frac{u}{2}W_0\left(-\frac{1}{2^{2/u}e}\right)}\right] \tag{13}$$

$$\omega_b = \frac{\omega_0}{2}\left[\sqrt{-\frac{u}{2}W_{-1}\left(-\frac{1}{2^{2/u}e}\right)} - \sqrt{-\frac{u}{2}W_0\left(-\frac{1}{2^{2/u}e}\right)}\right]. \tag{14}$$

In this section, we review the frequency characteristics of the GSW [26] and use them to derive an analytical expression for the GSW. In Section III, we propose an nth Fourier spectrum analysis algorithm and build the mathematical relationship between the frequency characteristics and the statistical properties of GSW. The statistical properties of the field signal can be used as an initial frequency analysis parameter, and the derived mathematical relationship can help us derive the corresponding GSW expression.

III. Statistical Properties of the nth Power Spectrum

Spectrum analysis of signals typically involves calculating the amplitude and power spectra, which are the first and second powers of the Fourier spectrum, respectively. If we extend this concept to the nth power spectrum and apply it to the spectrum analysis of the GSW, we can obtain the nth power Fourier spectra of the GSW as follows:

$$|\Phi^{(u)}(\omega)|^n = \left(\frac{u}{2}\right)^{-\frac{nu}{2}}\frac{\omega^{nu}}{\omega_0^{nu}}\exp\left(-\frac{n\omega^2}{\omega_0^2} + \frac{nu}{2}\right) = \left(\frac{2}{u}\right)^{\frac{nu}{2}}\frac{\omega^{nu}}{\omega_0^{nu}}\exp\left(-\frac{n\omega^2}{\omega_0^2} + \frac{nu}{2}\right) \tag{15}$$

where we only need to consider $\omega \ge 0$ and $u > 0$. If we set n to 1, the expression in (15) reduces to the amplitude spectrum of the GSW, as expressed in (4). If we set n to 2, the expression in (15) reduces to the power spectrum of the GSW.

Define the three definite integrals D_{I}, D_{II}, and D_{III} as follows (they are derived in the Appendix):

$$D_{\mathrm{I}} = \int_0^\infty |\Phi^{(u)}(\omega)|^n d\omega = \left(\frac{2}{nu}\right)^{\frac{nu}{2}}\frac{\exp\left(\frac{nu}{2}\right)\omega_0}{2\sqrt{n}}\Gamma\left(\frac{nu}{2}+\frac{1}{2}\right) \tag{16}$$

$$D_{\mathrm{II}} = \int_0^\infty \omega|\Phi^{(u)}(\omega)|^n d\omega = \left(\frac{2}{nu}\right)^{\frac{nu}{2}}\frac{u\omega_0^2\exp\left(\frac{nu}{2}\right)}{4}\Gamma\left(\frac{nu}{2}\right) \tag{17}$$

$$D_{\mathrm{III}} = \int_0^\infty (\omega-\omega_m)^2|\Phi^{(u)}(\omega)|^n d\omega = \left(\frac{2}{nu}\right)^{\frac{nu}{2}}\frac{\omega_0^3\exp\left(\frac{nu}{2}\right)}{4}\left[\frac{nu+1}{n\sqrt{n}}\Gamma\left(\frac{nu}{2}+\frac{1}{2}\right) - \frac{u^2\sqrt{n}\Gamma^2\left(\frac{nu}{2}\right)}{2\Gamma\left(\frac{nu}{2}+\frac{1}{2}\right)}\right]. \tag{18}$$

The mean frequency of the nth power spectrum of the GSW can be analytically expressed as follows:

$$\omega_{n,m} = \frac{\int_0^\infty \omega|\Phi^{(u)}(\omega)|^n d\omega}{\int_0^\infty |\Phi^{(u)}(\omega)|^n d\omega} = \frac{D_{\mathrm{II}}}{D_{\mathrm{I}}} = \frac{u\sqrt{n}\omega_0}{2}\frac{\Gamma\left(\frac{nu}{2}\right)}{\Gamma\left(\frac{nu}{2}+\frac{1}{2}\right)} \tag{19}$$

and the standard deviation is

$$\omega_{n,\sigma} = \left[\frac{\int_0^\infty (\omega-\omega_m)^2|\Phi^{(u)}(\omega)|^n d\omega}{\int_0^\infty |\Phi^{(u)}(\omega)|^n d\omega}\right]^{\frac{1}{2}} = \sqrt{\frac{D_{\mathrm{III}}}{D_{\mathrm{I}}}} = \frac{\omega_0}{\sqrt{2}}\sqrt{u+\frac{1}{n}-\frac{n}{2}\left[\frac{n\Gamma\left(\frac{nu}{2}\right)}{\Gamma\left(\frac{nu}{2}+\frac{1}{2}\right)}\right]^2}. \tag{20}$$

It is worth noting here that when $n = 2$, $\omega_{n,m}$ should be expressed as follows:

$$\omega_{2,m} = \frac{u\Gamma(u)}{\sqrt{2}\Gamma\left(u+\frac{1}{2}\right)}\omega_0 \tag{21}$$

and the standard deviation is

$$\omega_{2,\sigma} = \frac{\omega_0}{\sqrt{2}}\sqrt{u+\frac{1}{2}-\left[\frac{n\Gamma(u)}{\Gamma\left(u+\frac{1}{2}\right)}\right]^2} \tag{22}$$

which are the statistical property expressions derived based on the power spectrum of the GSW and the same as (27) and (28) in Wang's literature [26].

With (5), (13), (14), (19), and (20), we could set up the frequency coefficients $[\beta_p(u), \beta_c(u), \beta_b(u), \beta_m(u,n), \beta_\sigma(u,n)]^{\mathrm{T}}$,

of which the presentation is

$$\begin{bmatrix}\omega_p\\ \omega_c\\ \omega_b\\ \omega_{n,m}\\ \omega_{n,\sigma}\end{bmatrix} = \omega_0 \begin{bmatrix}\beta_p(u)\\ \beta_c(u)\\ \beta_b(u)\\ \beta_m(u,n)\\ \beta_\sigma(u,n)\end{bmatrix} = \omega_0 \begin{bmatrix}\sqrt{\frac{u}{2}}\\ \frac{1}{2}\left[\sqrt{-\frac{u}{2}W_{-1}\left(-\frac{1}{2^{2/u}e}\right)}+\sqrt{-\frac{u}{2}W_0\left(-\frac{1}{2^{2/u}e}\right)}\right]\\ \frac{1}{2}\left[\sqrt{-\frac{u}{2}W_{-1}\left(-\frac{1}{2^{2/u}e}\right)}-\sqrt{-\frac{u}{2}W_0\left(-\frac{1}{2^{2/u}e}\right)}\right]\\ \frac{\sqrt{nu}\Gamma\left(\frac{nu}{2}\right)}{2\Gamma\left(\frac{nu}{2}+\frac{1}{2}\right)}\\ \frac{1}{\sqrt{2}}\sqrt{\frac{1}{n}+u-\frac{n}{2}\left[\frac{u\Gamma\left(\frac{nu}{2}\right)}{\Gamma\left(\frac{nu}{2}+\frac{1}{2}\right)}\right]^2}\end{bmatrix}. \tag{23}$$

Equation (23) establishes the explicit mathematical relationship between the analytic frequency characteristics (ω_p, ω_c, and ω_b) and the statistical properties ($\omega_{n,m}$ and $\omega_{n,\sigma}$) based on the nth power Fourier spectrum of the GSW. It is important to note that the analytic frequency characteristics are not the functions of n and they are not first proposed in this article. They can be found in Wang's literature [26]. The statistical frequency coefficients $\beta_m(u,n)$ and $\beta_\sigma(u,n)$ are the functions of u and n. This means that our proposed approach allows the use of any power Fourier spectrum, such as, but not limited to, the amplitude spectrum ($n = 1$) or power spectrum ($n = 2$), to estimate the analytic frequency characteristics of the GSW.

As expected, the introduction of parameter n allows us to observe rich variations in the frequency coefficient trends, as shown in Fig. 1. The frequency characteristic coefficients [$\beta_p(u)$, $\beta_c(u)$, and $\beta_b(u)$] are depicted by solid curves in different colors, while the statistical frequency coefficients ($\beta_m(u,n)$ and $\beta_\sigma(u,n)$) are depicted by dotted curves.

To demonstrate the influence of different values of n on the statistical frequency coefficient, we plotted the frequency coefficient curves for n = 1.0, 1.5, 2.0, 2.5, and 3.0 as dotted curves with varying intervals in Fig. 1. From these curves, we can draw the following conclusions.

1) All the frequency coefficients are positively correlated with u. The statistical frequency coefficients are negatively correlated with n. As the value of n increases, the distance between the dotted curves decreases gradually, indicating that the negative correlation decreases with increasing n.
2) The curve of the central frequency coefficient $\beta_c(u)$ falls within the region of the curves of the mean frequency coefficient $\beta_m(u,n)$. This indicates that the mean frequency $\omega_{n,m}$ obtained from the nth power spectrum is approximately equal to the central frequency ω_c. From Fig. 1, we can see that the central frequency coefficient is closer to the mean frequency coefficient when $n = 2.0$ (power spectrum) than when $n = 1.5$. Similarly, the mean frequency estimated from the power spectrum is closer to the central frequency than the one obtained from the amplitude spectrum ($n = 1.0$) [26], [35]. Our proposed approach allows us to determine the exact value of n at which the mean frequency is equal to the central frequency, but we do not include this here.
3) All the frequency coefficient curves calculated from the nth power spectrum have the same trends and relative relationship to each other, including those obtained from the power spectrum [26]. This means that the different power degrees of the spectrum do not alter the variation trend of different frequency parameters, but the weight relationship among them is different. As a result, our proposed method can comprehensively analyze the input signal by analyzing the Fourier spectrum of the signal with different powers and using frequency parameters with varying relationships of weight, making the frequency analysis method more robust.

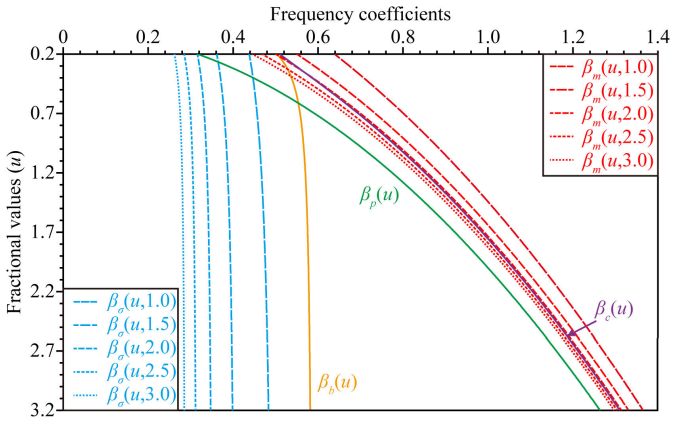

Fig. 1. Frequency coefficients $\beta_p(u)$, $\beta_c(u)$, $\beta_b(u)$, $\beta_m(u,n)$, and $\beta_\sigma(u,n)$ versus the power value of n and the fractional value of u.

IV. Weighting Algorithm of the nth Power Fourier Spectrum

To analyze the seismic data, we need to determine the range of values for the variable n to obtain the nth spectrum of the seismic signals. Then, we can use (18) and (19) to calculate the mean frequency and its deviation for the spectrum. Finally, using (23), we can calculate the ratio of the standard deviation to the mean frequency with respect to nu. The resulting ratio can be expressed as follows:

$$\frac{\omega_{n,\sigma}^2}{\omega_{n,m}^2} = \frac{(1+nu)}{nu}\left[\frac{\Gamma\left(\frac{nu}{2}+\frac{1}{2}\right)}{\sqrt{\frac{nu}{2}}\Gamma\left(\frac{nu}{2}\right)}\right]^2 - 1. \tag{24}$$

From which, the fractional value u of the Gaussian function could be solved using either a simple iterative method or an asymptotic series method [26]. After obtaining the value of u, the next step is to determine the reference frequency ω_0 to construct the desired GSW. However, it is essential to consider multiple frequency parameters to avoid errors caused by using a single frequency parameter. Therefore, the reference frequency ω_0 can be estimated using the following approach:

$$\omega_0 = \sqrt{\frac{2n}{1+nu}\left(\omega_{n,m}^2+\omega_{n,\sigma}^2\right)} \tag{25}$$

where the mean frequency $\omega_{n,m}$ and the deviation $\omega_{n,\sigma}$ are both used to help minimize the potential deviation when calculating the reference frequency ω_0.

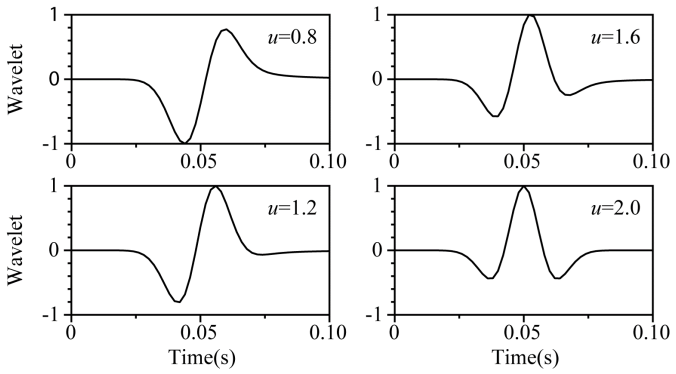

Fig. 2. GSWs defined by different fractional derivatives of a Gaussian function.

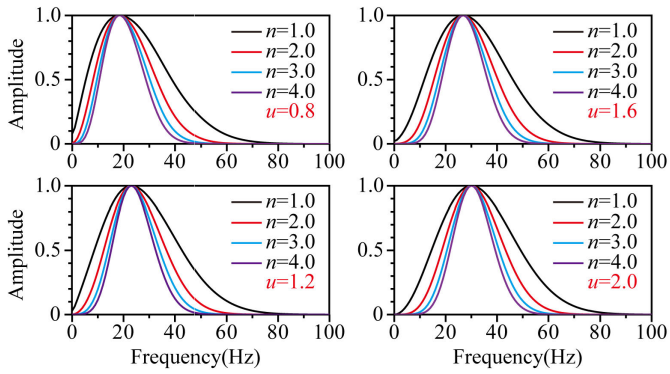

Fig. 3. Comparison of the nth power spectra of GSWs.

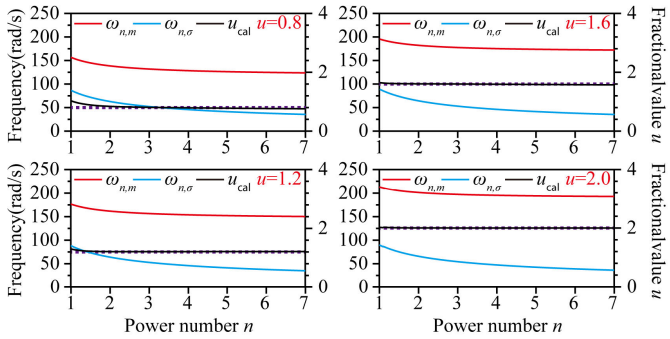

Fig. 4. Statistical properties ($\omega_{n,m}$ and $\omega_{n,\sigma}$) and u_{cal} calculated by the nth Fourier spectra of the ideal GSW.

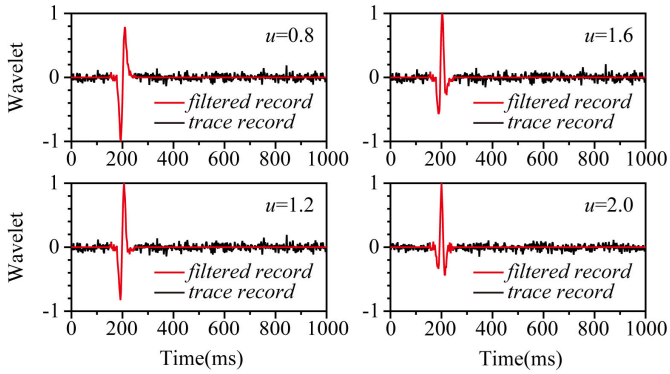

Fig. 5. Trace record synthesized with GSWs (including the Gaussian noise with an SNR of 15) and the filtered record by a cosine-square tapering.

In field seismic exploration, it is common for the seismic record to contain noise, affecting the accuracy of frequency characteristics in the signal spectrum. The frequency estimation results based on the amplitude spectrum or power spectrum, which is a single power of the Fourier spectrum, are often one-sided and may not be reliable.

Therefore, it is necessary to weight the calculated fractional value u_{cal} by different nth Fourier spectra to obtain a weighted fractional value u_{ave}. Using this weighted value, u_{ave} can often provide better robustness and noise immunity when calculating the reference frequency ω_0 and predicting the GSW.

V. Numerical Experiments

A. Frequency Analysis of Ideal GSWs

To demonstrate the effectiveness of the proposed method, we first utilize different fractional derivatives of a Gaussian function to construct the GSW, as shown in Fig. 2. In this figure, the fraction u ranges from 0.6 to 2.0. By changing the value of the fractional derivative of the Gaussian function, we can obtain wavelets with different phases. We then perform the GSW's Fourier transform and calculate the complex data's modulus to the nth power to bring the nth Fourier spectrum of the GSW. It is easy to infer that as n increases, the shape of the Fourier spectrum will be progressively narrower and more focused around the peak frequency. In Fig. 3, we show the nth power of the Fourier spectra of the GSW with a reference frequency of $\omega_0 = 60\pi$, which illustrates this phenomenon more clearly.

Using the nth Fourier spectra data, we can calculate the mean frequency $\omega_{n,m}$ and standard deviation $\omega_{n,\sigma}$ using (18) and (19), and then utilize (24) to calculate the fractional derivative u, as shown in Fig. 4. For GSWs of different phases, the calculated value of u_{cal} remains fairly constant as n changes, indicating that the correct fractional derivative u of the Gaussian function can be accurately calculated under ideal conditions, without noise in the seismic data.

B. Noise Immunity Test

To further examine the noise immunity of the proposed approach, we start with a synthesized first-arrival record using the GSW with a reference frequency of $\omega_0 = 60\pi$, as mentioned in Section V-A. We then add Gaussian noise with signal-to-noise ratios (SNRs) of 15 and 20. The noise-containing data are shown by the solid black curves in Figs. 5 and 6. To simulate the actual workflow, we pick up the first arrival based on the travel time and apply a cosine-square tapering to suppress unwanted seismic signals that are not part of the first arrival. The seismic signals after this processing are shown as solid red curves in Figs. 5 and 6.

We also perform nth Fourier spectrum calculation on the above noise-containing first-arrival records (synthesized by the GSW with $u = 2.0$). The results are shown by the solid red (SNR = 15) and blue (SNR = 20) curves in Fig. 7. For comparison, we also include the nth Fourier spectrum curves of the GSW without noise by the solid black curves in Fig. 7.

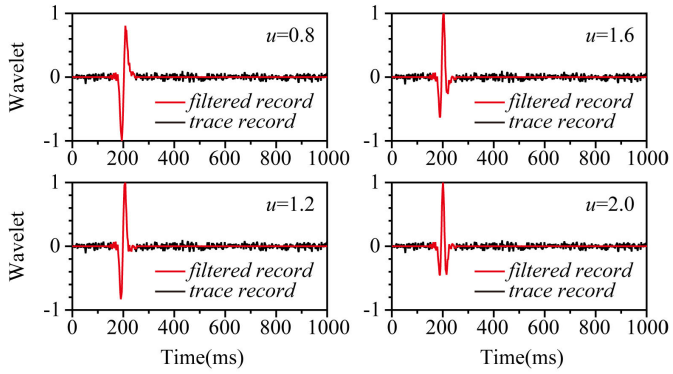

Fig. 6. Trace record synthesized with GSWs (including the Gaussian noise with an SNR of 20) and the filtered record by a cosine-square tapering.

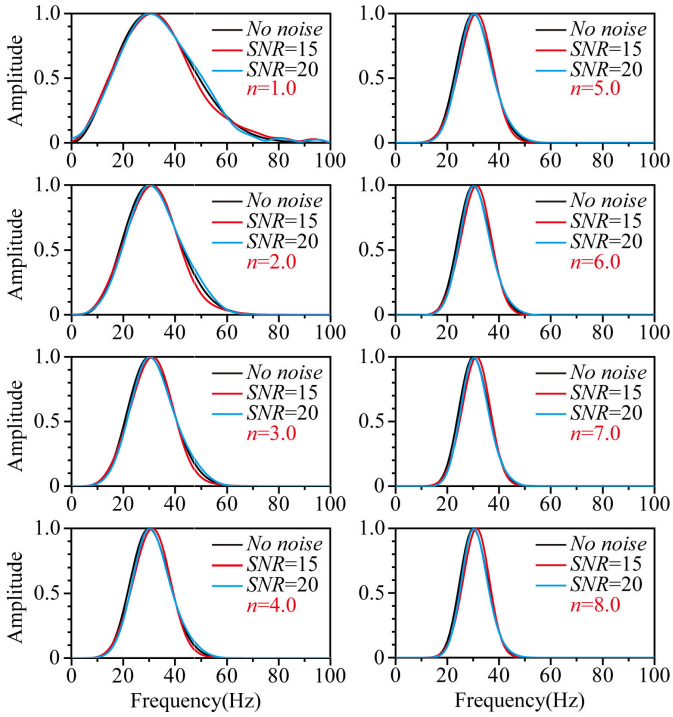

Fig. 7. nth Fourier spectra of the filtered noise-containing (SNR=15 and 20) and noise-free first-arrival records.

The Fourier spectra of the picked first arrivals with Gaussian noise are distorted compared to the noise-free synthetic seismic records. When n is relatively small, the energy in the Fourier spectrum exhibits a "defocusing" trend, meaning that the effective frequency band has a very small proportion of energy. The effect of noise on each Fourier spectrum is more pronounced, making it difficult to obtain accurate frequency information and predict the GSW using the Fourier spectra of a smaller power number. However, when n is relatively large, the corresponding nth Fourier spectra exhibit a "focusing" phenomenon. As a result, there is no significant difference in the shape between the nth Fourier spectra of noise-containing and noise-free first-arrival records. However, as n increases, the contribution of low- and high-frequency components in the signals is significantly reduced, and the frequency information of the "focus region" near the peak frequency does not fully represent all the frequency characteristics of the first-arrival

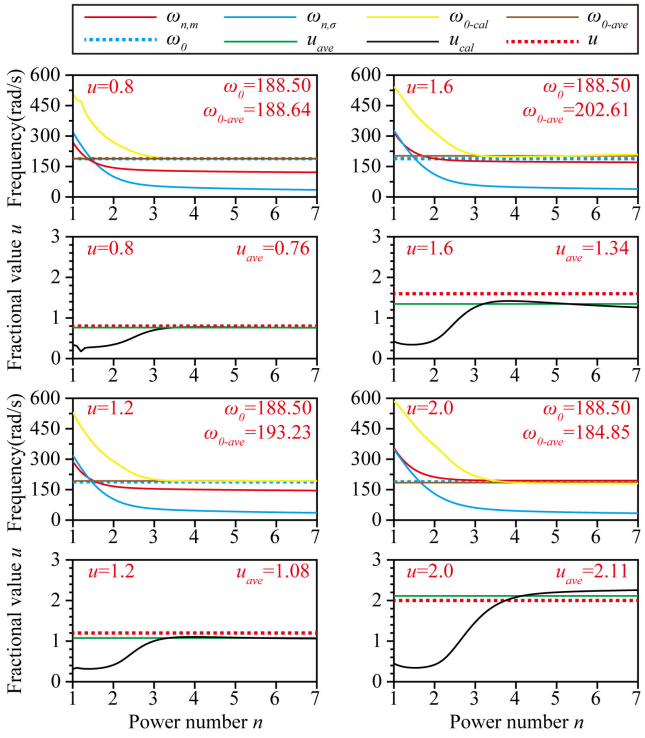

Fig. 8. Frequency parameters calculated by the nth Fourier spectra of the filtered noise-containing (SNR = 15) first-arrival records.

recordings. Therefore, relying solely on a specific n to obtain the nth Fourier spectrum and the calculated frequency parameter is not as reliable as one might think. To verify this point, we plot ω_σ, ω_m, and u_{cal} calculated from the nth Fourier spectra for different n values, as shown in Fig. 8 (SNR = 15) and Fig. 9 (SNR = 20). In these figures, we can see that the calculated ω_m, ω_d, and u tend to change with the change of n. When n is small, the "defocusing" mentioned above leads to larger values of ω_σ and ω_m, which in turn leads to a calculated u_{cal} value (shown as the solid black curves in Figs. 8 and 9) that is less than the correct u value (shown as the dotted red curves in Figs. 8 and 9). As the value of n increases, the calculated u_{cal} value gradually becomes stable. However, there is still a discrepancy with the correct u, and we cannot arbitrarily assume that the higher the value of n, the more accurate the calculation is. Therefore, using an average of u_{cal} values calculated from different nth Fourier spectra, known as u_{ave}, can improve the robustness and noise immunity of the GSW estimation method.

In this test, we use the range of n from 3.0 to 7.0 to calculate the average weighting u_{ave}. It is worth noting that the selection of the range of n is an empirical parameter, and the same range is used in the subsequent experiments in this article. u_{ave} is shown by the solid green curves in Figs. 8 and 9. It can be seen that the weighting u_{ave} value is very close to the correct value of u, even when the data includes noise. The calculation accuracy is significantly higher than conventionally used the amplitude spectrum ($n = 1.0$) or power spectrum ($n = 2.0$) . While it may be possible to find a specific value of n that results in a calculated u_{cal} value closest to the correct value of u for each trace record

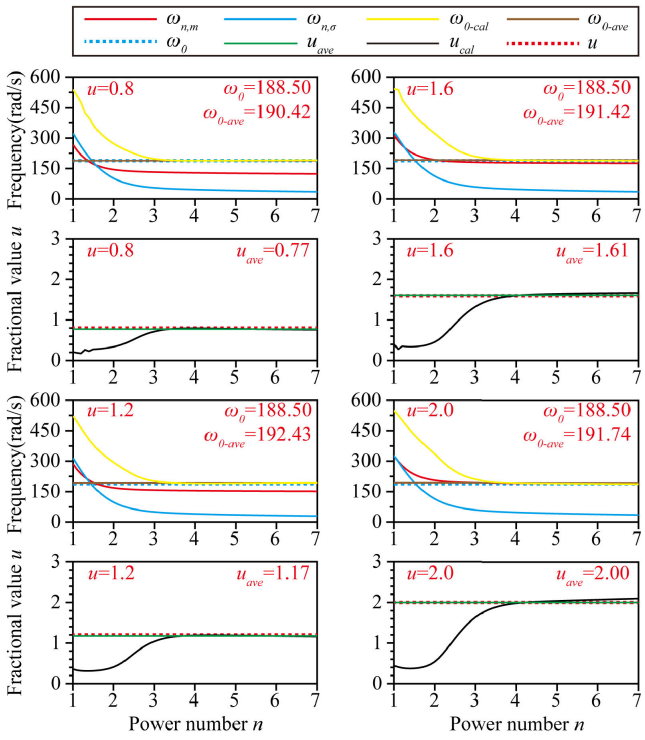

Fig. 9. Frequency parameters calculated by the nth Fourier spectra of the filtered noise-containing (SNR = 20) first-arrival records.

data, it is not possible to predict this specific value of n in the actual workflow. Therefore, the weighting u_{ave} method proposed in this article often achieves higher precision and robustness. Next, we substitute the u_{ave} into (25) and continue to calculate ω_0 from the nth Fourier spectrum. The results are shown by the solid yellow curves in Figs. 8 and 9. Similarly, it is challenging to obtain relatively accurate ω_0 by relying on the Fourier spectrum of a single power degree. Therefore, it is also necessary to perform the weighting calculation on ω_0. In this experiment, we again use the nth Fourier spectrum in the range of 3.0–7.0. The computed $\omega_{0-\text{cal}}$ is weighted proportionally to obtain $\omega_{0-\text{ave}}$, as shown by the solid brown curves in Figs. 8 and 9. The experimental results show that $\omega_{0-\text{ave}}$ obtained through weighting calculations is close to the theoretically correct value of ω_0.

By using the weighting u_{ave} and $\omega_{0-\text{ave}}$, along with the picked first-arrival time τ_0, we construct the Fourier spectrum data according to (3) and perform the inverse Fourier transform to obtain the predicted time-domain seismic signals, as shown in Fig. 10. From this, we can see that the seismic record constructed using the GSW synthesized by the proposed method has a high correlation coefficient with the test data (parameter "c" in Fig. 10), demonstrating the effectiveness and strong noise resistance of the proposed method.

C. Field Signal Experiment

In this section, we test our approach using field VSP records. We select ten traces of pressure data from a VSP common shot gather, with ten receivers between depths of 750 and 840 m. Fig. 11 displays the ten trace records and the frequency

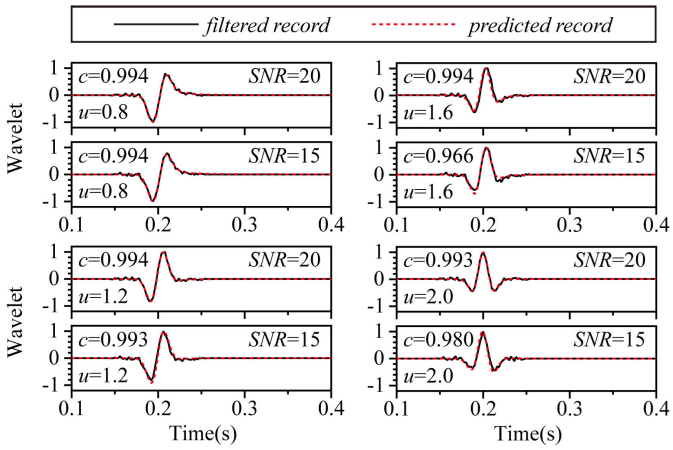

Fig. 10. Comparison between the synthetic noise-containing records and the predicted records with weighting u_{ave} and $\omega_{0-\text{ave}}$.

analysis results using the proposed method. From this, we can observe the following.

1) The waveforms between 250 and 400 ms including the first arrivals are shown in the "Wavelets" column. The solid gray curves represent the initial field trace records, while the solid black curves show the filtered trace records using a cosine-square tapering, suppressing unwanted seismic signals such as multiples and reflections. We compared the matching of the field signals and GSWs predicted using the amplitude spectrum, power spectrum, and the proposed method, shown as solid red, blue, and green curves, respectively. In this experiment, we still use the range of n from 3.0 to 7.0 for the weighting calculation of the Fourier spectra. The GSW calculated using the amplitude or power spectrum can match well with the field signals. The method proposed in this article avoids the contingency of frequency estimation by using the above two Fourier spectra in the weighting calculation of different power Fourier spectra, which theoretically performs better than the first two.
2) In the "Correlation" column, we also plotted the correlation curves between the filtered trace record and the GSW calculated using the amplitude, power spectrum, and the proposed method. These correlation coefficients further verify the points made above.
3) From the "ω_0 and ω_m" and "u" columns, we can see a high correlation between ω_m and u regardless of which Fourier spectrum is used, which is similar to the conclusion reached in Wang's article [26]. Additionally, the values of u calculated using the amplitude and power spectra are smaller than the proposed method, which is more accurate based on the matching between the GSW and the field signals. Lastly, the differences between ω_0 calculated using the amplitude, power, and nth spectra are not as significant as in the previous test. The author believes that this is because the noise type in the field trace record is different from the previous test.

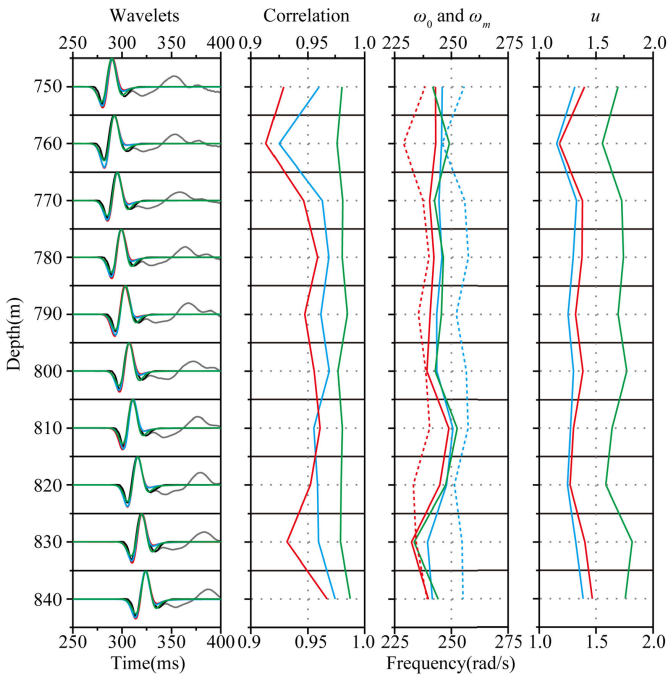

Fig. 11. GSWs and frequency analysis comparisons from the amplitude, power, and nth Fourier spectra of the field VSP records.

D. Necessary Preprocessing

To clearly express the proposed method, we have avoided some preprocessing steps by selecting a safe window in the above experiments. However, it is important to note that the proposed method is a type of spectral fitting method that is sensitive to the shape of the Fourier spectrum [25]. This means that some of the Earth's response may be unavoidable and could potentially influence the statistical properties inferred from field data. Therefore, in actual application scenarios, it is necessary to apply some preprocessing to the input signal to make it suitable for use with the proposed method.

For example, when using the proposed method for stable Q analysis on VSP data (a typical application scenario [6]), effective first-arrival extraction processing is essential for wavelet estimation. To obtain the downgoing wavetrains, we should first apply median filtering and then use a cosine-square taper according to the first-arrival travel time to suppress late arrivals, which are mostly made up of waveforms of multiples generated from the free surface [6], [26]. Only then can we use the effective first-arrival signal with the proposed method. In other seismic data application scenarios, there are also unique preprocessing steps, which will not be described in this article.

VI. Conclusion and Discussion

The frequency analysis method based on the amplitude or power spectrum can be used to construct the GSW matching well with seismic recording signals. The proposed approach builds upon this by using the nth power Fourier spectra to compute the frequency properties of the GSW, which is a theoretical extension of the power number of the Fourier spectrum from 1 or 2 to an arbitrary value. This method provides analytical expressions for the frequency properties of the GSW, such as the central frequency, the bandwidth, the mean frequency, and the deviation, creating a more holistic and straightforward relation between the frequency characteristics and statistical properties. Based on this, the frequency properties of the GSW can be seen as a function of both the fractional value of u and the power value of n, rather than just being related to the value of u. The proposed frequency analysis technique based on the nth power Fourier spectra is not contradictory to the method based on the power spectrum that has been published on some literatures [26], [35], [38]. In fact, it provides a more comprehensive frequency analysis strategy. The proposed method can achieve higher robustness and noise resistance by weighting the fractional derivatives u_{ave} of the Gaussian function, as both theoretical and field trace data have shown.

The GSW is a flexible method for defining wavelets. It can be used not only to extract seismic wavelets from first-arrival data, but also to play a crucial role in the seismic wavelet extraction method based on reflected data. However, current methods for estimating frequency parameters still rely on the amplitude spectrum or power spectrum [24], [25], [39]. The proposed plan has the potential to be extended to these methods and provide more stable and accurate algorithm support. This is also the future direction of this article.

Appendix
Derivation of the Definite Integrals D_{I}, D_{II}, and D_{III}

First, we need to define $x = ((n)^{1/2}\omega/\omega_0)$ and $y = x^2 = (n\omega^2/\omega_0^2)$. According to the concept and property of the Gamma function, we can obtain

$$\int_0^\infty x^{nu}\exp(-x^2)dx = \frac{1}{2}\Gamma\left(\frac{nu}{2}+\frac{1}{2}\right) \tag{A.1}$$

$$\int_0^\infty y^{\frac{nu+1}{2}}\exp(-y)dy = \Gamma\left(\frac{nu+1}{2}+1\right) = \frac{nu+1}{2}\Gamma\left(\frac{nu+1}{2}\right). \tag{A.2}$$

The derivation process of (16) is as follows:

$$\begin{aligned} D_{\text{I}} &= \int_0^\infty |\Phi^{(u)}(\omega)|^n d\omega \\ &= \int_0^\infty \left(\frac{2}{u}\right)^{\frac{nu}{2}} \frac{\omega^{nu}}{\omega_0^{nu}}\exp\left(-\frac{n\omega^2}{\omega_0^2}+\frac{nu}{2}\right)d\omega \\ &= \left(\frac{2}{nu}\right)^{\frac{nu}{2}} \frac{\exp\left(\frac{nu}{2}\right)\omega_0}{\sqrt{n}} \int_0^\infty \left(\frac{\sqrt{n}\omega}{\omega_0}\right)^{nu} \cdot \\ &\quad \exp\left[-\left(\frac{\sqrt{n}\omega}{\omega_0}\right)^2\right] d\left(\frac{\sqrt{n}\omega}{\omega_0}\right) \\ &= \left(\frac{2}{nu}\right)^{\frac{nu}{2}} \frac{\exp\left(\frac{nu}{2}\right)\omega_0}{\sqrt{n}} \int_0^\infty x^{nu}\exp(-x^2)dx \\ &= \left(\frac{2}{nu}\right)^{\frac{nu}{2}} \frac{\exp\left(\frac{nu}{2}\right)\omega_0}{2\sqrt{n}}\Gamma\left(\frac{nu}{2}+\frac{1}{2}\right). \end{aligned} \tag{A.3}$$

The derivation process of (17) is as follows:

$$\begin{aligned} D_{\mathrm{II}} &= \int_0^{\infty} \omega |\Phi^{(u)}(\omega)|^n d\omega \\ &= \left(\frac{2}{u}\right)^{\frac{nu}{2}} \exp\left(\frac{nu}{2}\right) \int_0^{\infty} \omega \left(\frac{\omega}{\omega_0}\right)^{nu} \cdot \\ &\quad \exp\left[-\left(\frac{\sqrt{n}\omega}{\omega_0}\right)^2\right] d\omega \\ &= \left(\frac{2}{nu}\right)^{\frac{nu}{2}} \frac{\omega_0^2 \exp\left(\frac{nu}{2}\right)}{2n} \cdot \\ &\quad \int_0^{\infty} \left(\frac{n\omega^2}{\omega_0^2}\right)^{\frac{nu}{2}} \exp\left(-\frac{n\omega^2}{\omega_0^2}\right) d\left(\frac{n\omega^2}{\omega_0^2}\right) \\ &= \left(\frac{2}{nu}\right)^{\frac{nu}{2}} \frac{\omega_0^2 \exp\left(\frac{nu}{2}\right)}{2n} \int_0^{\infty} y^{\frac{nu}{2}} \exp(-y) dy \\ &= \left(\frac{2}{nu}\right)^{\frac{nu}{2}} \frac{\omega_0^2 \exp\left(\frac{nu}{2}\right)}{2n} \Gamma\left(\frac{nu}{2}+1\right) \\ &= \left(\frac{2}{nu}\right)^{\frac{nu}{2}} \frac{u\omega_0^2 \exp\left(\frac{nu}{2}\right)}{4} \Gamma\left(\frac{nu}{2}\right). \end{aligned} \tag{A.4}$$

The derivation process of (18) is as follows:

$$\begin{aligned} D_{\mathrm{III}} &= \int_0^{\infty} (\omega - \omega_m)^2 |\Phi^{(u)}(\omega)|^n d\omega \\ &= \int_0^{\infty} \omega^2 |\Phi^{(u)}(\omega)|^n d\omega \\ &\quad - \int_0^{\infty} 2\omega\omega_m |\Phi^{(u)}(\omega)|^n d\omega \\ &\quad + \int_0^{\infty} {\omega_m}^2 |\Phi^{(u)}(\omega)|^n d\omega \\ &= \int_0^{\infty} \omega^2 |\Phi^{(u)}(\omega)|^n d\omega - 2\omega_m D_{\mathrm{II}} + {\omega_m}^2 D_{\mathrm{I}}. \end{aligned} \tag{A.5}$$

To further deduce (A.5), we need to solve the following definite integral:

$$\begin{aligned} &\int_0^{\infty} \omega^2 |\Phi^{(u)}(\omega)|^n d\omega \\ &= \int_0^{\infty} \omega^2 \left(\frac{2}{u}\right)^{\frac{nu}{2}} \frac{\omega^{nu}}{\omega_0^{nu}} \exp\left(-\frac{n\omega^2}{\omega_0^2} + \frac{nu}{2}\right) d\omega \\ &= \left(\frac{2}{nu}\right)^{\frac{nu}{2}} \frac{\omega_0^3 \exp\left(\frac{nu}{2}\right)}{2n\sqrt{n}} \cdot \\ &\quad \int_0^{\infty} \left(\frac{n\omega^2}{\omega_0^2}\right)^{\frac{nu+1}{2}} \exp\left(-\frac{n\omega^2}{\omega_0^2}\right) d\left(\frac{n\omega^2}{\omega_0^2}\right) \\ &= \left(\frac{2}{nu}\right)^{\frac{nu}{2}} \frac{\omega_0^3 \exp\left(\frac{nu}{2}\right)}{2n\sqrt{n}} \int_0^{\infty} y^{\frac{nu+1}{2}} exp(-y) dy \\ &= \left(\frac{2}{nu}\right)^{\frac{nu}{2}} \frac{\omega_0^3 \exp\left(\frac{nu}{2}\right)}{2n\sqrt{n}} \Gamma\left(\frac{nu+1}{2}+1\right) \\ &= \left(\frac{2}{nu}\right)^{\frac{nu}{2}} \frac{(nu+1)\omega_0^3 \exp\left(\frac{nu}{2}\right)}{4n\sqrt{n}} \Gamma\left(\frac{nu+1}{2}\right). \end{aligned} \tag{A.6}$$

Take (A.3), (A.4), and (A.6) into equation (A.5), D_{III} could be expressed as follows:

$$\begin{aligned} D_{\mathrm{III}} &= \left(\frac{2}{nu}\right)^{\frac{nu}{2}} \frac{\omega_0^3 \exp\left(\frac{nu}{2}\right)}{4} \cdot \\ &\quad \left[\frac{nu+1}{n\sqrt{n}} \Gamma\left(\frac{nu}{2}+\frac{1}{2}\right) - \frac{u^2\sqrt{n}\Gamma^2\left(\frac{nu}{2}\right)}{2\Gamma\left(\frac{nu}{2}+\frac{1}{2}\right)}\right]. \end{aligned} \tag{A.7}$$

REFERENCES

[1] N. Ricker, "Further developments in the wavelet theory of seismogram structure," *Bull. Seismol. Soc. Amer.*, vol. 33, no. 3, pp. 197–228, 1943.

[2] N. Ricker, "Wavelet functions and their polynomials," *Geophysics*, vol. 9, no. 3, pp. 314–323, Jul. 1944.

[3] N. Ricker, "The form and laws of propagation of seismic wavelets," *Geophysics*, vol. 18, no. 1, pp. 10–40, 1953.

[4] J. W. J. Hosken, "Ricker wavelets in their various guises," *1st Break*, vol. 6, no. 1, pp. 1–10, Jan. 1988.

[5] Y. Wang, "Q analysis on reflection seismic data," *Geophys. Res. Lett.*, vol. 31, no. 17, 2004, Art. no. L17606.

[6] Y. Wang, "Stable q analysis on vertical seismic profiling data," *Geophysics*, vol. 79, no. 4, pp. D217–D225, Jul. 2014.

[7] N. Wang, G. Xing, T. Zhu, H. Zhou, and Y. Shi, "Propagating seismic waves in VTI attenuating media using fractional viscoelastic wave equation," *J. Geophys. Res., Solid Earth*, vol. 127, no. 4, Apr. 2022, Art. no. Art. no. e2021JB023280.

[8] Z.-M. Ren, X. Dai, and Q.-Z. Bao, "Source wavefield reconstruction based on an implicit staggered-grid finite-difference operator for seismic imaging," *Petroleum Sci.*, vol. 19, no. 5, pp. 2095–2106, Oct. 2022.

[9] L. Song, Y. Shi, W. Liu, and Q. Zhao, "Elastic reverse time migration for weakly illuminated structure," *Appl. Sci.*, vol. 12, no. 10, p. 5264, May 2022.

[10] X.-B. Guo, H. Liu, and Y. Shi, "Modified interferometric imaging condition for reverse-time migration," *Explor. Geophys.*, vol. 49, no. 2, pp. 202–212, Apr. 2018.

[11] W. Zhang and Y. Shi, "Imaging conditions for elastic reverse time migration," *Geophysics*, vol. 84, no. 2, pp. S95–S111, Mar. 2019.

[12] W. Zhang, J. Gao, Z. Gao, and Y. Shi, "2D and 3D amplitude-preserving elastic reverse time migration based on the vector-decomposed P- and S-wave records," *Geophys. Prospecting*, vol. 68, no. 9, pp. 2712–2737, 2020.

[13] Z. Ren, Q. Bao, and S. Xu, "Memory-efficient source wavefield reconstruction and its application to 3D reverse time migration," *Geophysics*, vol. 87, no. 1, pp. S21–S34, Jan. 2022.

[14] W. Zhang, J. Gao, Y. Cheng, C. Su, H. Liang, and J. Zhu, "3-D image-domain least-squares reverse time migration with L_1 norm constraint and total variation regularization," *IEEE Trans. Geosci. Remote Sens.*, vol. 60, 2022, Art. no. 5918714.

[15] X. Guo, H. Liu, Y. Shi, W. Wang, and Z. Zhang, "Improving waveform inversion using modified interferometric imaging condition," *Acta Geophys.*, vol. 66, no. 1, pp. 71–80, Feb. 2018.

[16] W. Zhang and J. Gao, "Deep-learning full-waveform inversion using seismic migration images," *IEEE Trans. Geosci. Remote Sens.*, vol. 60, pp. 1–18, 2021.

[17] Z. Ren, Q. Bao, and B. Gu, "Time-dispersion correction for arbitrary even-order lax-wendroff methods and the application on full-waveform inversion," *Geophysics*, vol. 86, no. 5, pp. T361–T375, Sep. 2021.

[18] E. Bianco, "Tutorial: Wavelet estimation for well ties," *Lead. Edge*, vol. 35, no. 6, pp. 541–543, Jun. 2016.

[19] L. R. Lines and S. Treitel, "Wavelets, well logs and Wiener filters," *1st Break*, vol. 3, no. 8, pp. 9–14, Aug. 1985.

[20] I. A. S. de Macedo and J. J. S. de Figueiredo, "On the seismic wavelet estimative and reflectivity recovering based on linear inversion: Well-to-seismic tie on a real data set from viking graben, North Sea," *Geophysics*, vol. 85, no. 5, pp. D157–D165, Sep. 2020.

[21] M. D. Sacchi and T. J. Ulrych, "Nonminimum-phase wavelet estimation using higher order statistics," *Lead. Edge*, vol. 19, no. 1, pp. 80–83, 2000.

[22] A. T. Walden and R. E. White, "Seismic wavelet estimation: A frequency domain solution to a geophysical noisy input-output problem," *IEEE Trans. Geosci. Remote Sens.*, vol. 36, no. 1, pp. 287–297, Jan. 1998.

[23] R. Zhang and Z. Deng, "A depth variant seismic wavelet extraction method for inversion of poststack depth-domain seismic data," *Geophysics*, vol. 83, no. 6, pp. R569–R579, Nov. 2018.

[24] S. Ker and Y. Le Gonidec, "Filtering of a Ricker wavelet induced by anelastic seismic wave propagation and reflection," *J. Geophys. Eng.*, vol. 17, no. 5, pp. 838–851, Sep. 2020.
[25] J. Zhang, X. Chen, W. Jiang, Y. Liu, and H. Xu, "Estimation of the depth-domain seismic wavelet based on velocity substitution and a generalized seismic wavelet model," *Geophysics*, vol. 87, no. 2, pp. R213–R222, Mar. 2022.
[26] Y. Wang, "Generalized seismic wavelets," *Geophys. J. Int.*, vol. 203, no. 2, pp. 1172–1178, Nov. 2015.
[27] Y. Rao, Y. Guo, and D. Xu, "Detecting Karst voids based on dominant frequencies of seismic profiles," *Pure Appl. Geophys.*, vol. 178, no. 8, pp. 3057–3067, Aug. 2021.
[28] D. Yang, J. Liu, J. Li, and D. Liu, "Q-factor estimation using bisection algorithm with power spectrum," *Geophysics*, vol. 85, no. 3, pp. V233–V248, 2020.
[29] H. H. Hardy, R. A. Beier, and J. D. Gaston, "Frequency estimates of seismic traces," *Geophysics*, vol. 68, no. 1, pp. 370–380, Jan. 2003.
[30] S. Huo, "Frequency estimates of seismic traces," *Geophysics*, vol. 80, no. 5, pp. V115–V118, 2015.
[31] S. S. Ahmad, R. J. Brown, A. Escalona, and B. O. Rosland, "Frequency-dependent velocity analysis and offset-dependent low-frequency amplitude anomalies from hydrocarbon-bearing reservoirs in the southern North Sea, Norwegian sector," *Geophysics*, vol. 82, no. 6, pp. N51–N60, 2017.
[32] A. J. Carter and J.-M. Kendall, "Attenuation anisotropy and the relative frequency content of split shear waves," *Geophys. J. Int.*, vol. 165, no. 3, pp. 865–874, Jun. 2006.
[33] J. H. Lambert, "Observationes variae in mathesin puram," *Acta Helvetica*, vol. 3, no. 1, pp. 128–168, 1758.
[34] R. M. Corless, G. H. Gonnet, D. E. G. Hare, D. J. Jeffrey, and D. E. Knuth, "On the LambertW function," *Adv. Comput. Math.*, vol. 5, no. 1, pp. 329–359, Dec. 1996.
[35] Y. Wang, "Frequencies of the Ricker wavelet," *Geophysics*, vol. 80, no. 2, pp. A31–A37, Mar. 2015.
[36] A. E. Barnes, "Instantaneous spectral bandwidth and dominant frequency with applications to seismic reflection data," *Geophysics*, vol. 58, no. 3, pp. 419–428, Mar. 1993.
[37] M. Caputo, "Linear models of dissipation whose Q is almost frequency independent—II," *Geophys. J. Int.*, vol. 13, no. 5, pp. 529–539, 1967.
[38] Y. Wang, "The Ricker wavelet and the Lambert W function," *Geophys. J. Int.*, vol. 200, no. 1, pp. 111–115, Jan. 2015.
[39] Y. Jiang, S. Cao, S. Chen, and D. Zheng, "A blind nonstationary deconvolution method for multichannel seismic data," *Explor. Geophys.*, vol. 52, no. 3, pp. 245–257, May 2021.

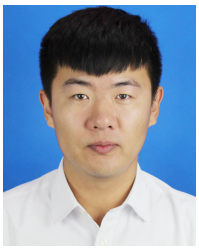

Xuan Ke was born in Anda, Heilongjiang, China, in 1989. He received the B.S. degree in geophysics, the M.S. degree in geological engineering, and the Ph.D. degree in geological resources and geological engineering from Northeast Petroleum University, Daqing, Heilongjiang, in 2012, 2015, and 2017, respectively.

He is currently a Visiting Scholar with the University of Alberta, Edmonton, AB, Canada. Since 2021, he has been an Associate Professor of the School of Earth Science. He has published more than ten articles and undertook five research projects about seismic imaging. His research interests include seismic wavefield simulation and reverse time migration.

Ying Shi received the Ph.D. degree in solid geophysics from the Institute of Geology and Geophysics, Chinese Academy of Sciences, Beijing, China, in 2010.

She was a Visiting Scholar with the Imperial College London, London, U.K., from 2014 to 2015. She is currently a Professor with the School of Earth Science. She has published more than 50 articles, of which 18 are indexed by Science Citation Index (SCI) and four are indexed by Engineering Index (EI). Her research interests include reverse time migration, full waveform inversion, multiple attenuations, seismic wave propagation, and complex structure imaging.

Dr. Shi was awarded the Longjiang Scholars Support Program in 2018 and the Fu Chengyi Youth Science and Technology Award in 2019.

Xiaofei Fu was born in Chifeng, Neimenggu, China, in 1973. He received the Ph.D. degree from the PetroChina Research Institute of Exploration and Development, Daqing, China, in 2007.

He is currently a Professor with the Institute of Unconventional Oil and Gas, Northeast Petroleum University, Daqing. He has published more than 90 articles, of which 19 are indexed by Science Citation Index (SCI) and 47 are indexed by Engineering Index (EI). His research interests include the integration of geology and geophysics.

Dr. Fu was awarded the Longjiang Scholars Support Program in 2012.

Liwei Song received the M.S. degree in nuclear technology and applications from Heilongjiang University, Harbin, China, in 2012, and the Ph.D. degree in geological resources and geological engineering from Northeast Petroleum University, Daqing, China, in 2018.

From 2018 to 2019, he was a Visiting Scholar with the University of Monash, Melbourne, VIC, Australia. He is currently a Lecturer with the School of Physics and Electronic Engineering, Northeast Petroleum University. His research interests include geophysical data processing, inverse problems, and deep learning.

Hongliang Jing was born in Suihua, Heilongjiang, China, in 1987. He received the master's degree in geophysics from Northeast Petroleum University, Daqing, Heilongjiang, in 2015.

Since 2015, he has been working with BGP Inc., CNPC, Zhuozhou, China. He is mainly engaged in seismic data processing and geophysical prospecting method research.

Jingbo Yang was born in Harbin, Heilongjiang, China, in 1988. He received the B.S. degree in geochemistry and the M.S. degree in geological engineering from Northeast Petroleum University, Daqing, Heilongjiang, in 2012 and 2015, respectively.

Since 2015, he has been working with China National Petroleum Corporation, Tarim Oilfield, Korla, China. He has obtained more than ten bureau-level awards, and he mainly engaged in geological exploration.

Zhen Zhang was born in Daqing, Heilongjiang, China, in 1989. He received the B.S. degree in geophysics and the M.S. degree in geological engineering from Northeast Petroleum University, Daqing, China, in 2012 and 2015, respectively.

Since 2015, he has been an Engineer with Tarim Oilfield, Korla, China. He has published more than ten articles. His research interests include seismic data processing and borehole seismic data processing.